We are IntechOpen, the world's leading publisher of Open Access books Built by scientists, for scientists

6,900
Open access books available

185,000
International authors and editors

200M
Downloads

Our authors are among the

154
Countries delivered to

TOP 1%
most cited scientists

12.2%
Contributors from top 500 universities

BOOK CITATION INDEX CLARIVATE ANALYTICS INDEXED

WEB OF SCIENCE™

Selection of our books indexed in the Book Citation Index in Web of Science™ Core Collection (BKCI)

Interested in publishing with us?
Contact book.department@intechopen.com

Matrix Cracking of Ceramic-Matrix Composites

Li Longbiao

Abstract

In this chapter, the matrix cracking of fiber-reinforced ceramic-matrix composites (CMCs) is investigated using the energy balance approach. The relationship between the matrix cracking stress, fiber and interface oxidation, and fiber failure is established. The effects of the fiber volume, interface shear stress and interface debonding energy, fiber failure, and oxidation temperature on the time-dependent matrix cracking stress are analyzed. The experimental matrix cracking stress of different fiber-reinforced CMCs is predicted using the present models.

Keywords: ceramic-matrix composites, matrix cracking, oxidation, interface shear stress

1. Introduction

Ceramic-matrix composites (CMCs) possess high specific strength and high specific modulus especially at elevated temperature and have already been applied in hot-section components in aeroengine [1]. However, at elevated temperature, the environment affects the mechanical performance of fiber-reinforced CMCs. The matrix cracking stress decreases with operation time due to the interface oxidation [2]. Many researchers performed investigations on matrix cracking of fiber-reinforced CMCs, i.e., the energy balance approach developed by Aveston et al. [3]; Budiansky et al. [4]; Rajan and Zok [5]; and Li [6, 7], and the fracture mechanics approach proposed by Marshall et al. [8], and McCartney [9]. At elevated temperature, the oxidative environment entered inside of fiber-reinforced CMCs through the microcrackings, and the lifetime is affected by the applied load and temperature [10, 11].

In this chapter, the effects of temperature, oxidation, and applied stress on the time-dependent matrix cracking stress of fiber-reinforced CMCs are investigated. The relationship between the matrix cracking stress, fiber and interface oxidation, and fiber failure is established. The effects of the fiber volume, interface shear stress and interface debonding energy, fiber failure, and oxidation temperature on the time-dependent matrix cracking stress are analyzed. The experimental matrix cracking stress of different fiber-reinforced CMCs are predicted.

2. Theoretical analysis

At elevated temperature, oxygen reacts with the interphase along the fiber length. The time-dependent interphase oxidation length can be determined using the following equation (11) [12].

$$\zeta = \varphi_1 \left[1 - \exp\left(-\frac{\varphi_2 t}{b}\right)\right] \tag{1}$$

where φ_1 and φ_2 are parameters dependent on temperature and described using the Arrhenius type laws and b is a delay factor considering the deceleration of reduced oxygen activity.

The oxidation of fiber is assumed to be controlled by diffusion of oxygen gas through matrix cracks. By assuming that the fracture toughness of the fibers remains constant and that the fiber strength σ_0 is related to the mean oxidized layer thickness, the time dependence of the fiber strength can be determined by the following equation (12).

$$\sigma_0(t) = \sigma_0, t \leq \frac{1}{k}\left(\frac{K_{IC}}{Y\sigma_0}\right)^4 \tag{2}$$

$$\sigma_0(t) = \frac{K_{IC}}{Y\sqrt[4]{kt}}, t > \frac{1}{k}\left(\frac{K_{IC}}{Y\sigma_0}\right)^4 \tag{3}$$

When the fiber breaks, the stress carried by the intact and broken fibers can be determined using the global load sharing (GLS) criterion by Eq. (4) [13].

$$\frac{\sigma}{V_f} = T[1 - P(T)] + \langle T_b \rangle P(T) \tag{4}$$

where V_f denotes the fiber volume fraction, T denotes the load carried by intact fibers, $\langle T_b \rangle$ denotes the load carried by broken fibers, and $P(T)$ denotes the fiber failure probability.

$$P(T) = \eta P_a(T) + (1 - \eta)P_b(T) + P_c(T) \tag{5}$$

where η denotes the oxidation fiber fraction in the oxidation region and $P_a(T)$, $P_b(T)$, and $P_c(T)$ denote the fracture probability of oxidized fibers and unoxidized fibers in the oxidation region and interface debonding region, respectively.

2.1 Downstream stresses

Figure 1 shows the composite under loading of a remote uniform applied stress of σ with a long matrix cracking. A unit cell is extracted from the composite to analyze the microstress field of the damaged fiber-reinforced CMCs, as shown in **Figure 2**. The fiber and matrix axial stress in the interface oxidation and debonding region can be determined using the following equation.

$$\sigma_f^D(z) = \begin{cases} T - \dfrac{2\tau_f}{r_f}z, z \in (0, \zeta) \\ T - \dfrac{2\tau_f}{r_f}\zeta - \dfrac{2\tau_i}{r_f}(z - \zeta), z \in (\zeta, l_d) \end{cases} \tag{6}$$

$$\sigma_m^D(z) = \begin{cases} 2\dfrac{V_f}{V_m}\dfrac{\tau_f}{r_f}z, z \in (0, \zeta) \\ 2\dfrac{V_f}{V_m}\dfrac{\tau_f}{r_f}\zeta + 2\dfrac{V_f}{V_m}\dfrac{\tau_i}{r_f}(z - \zeta), z \in (\zeta, l_d) \end{cases} \tag{7}$$

In the fiber/matrix interface bonding region, the fiber and matrix axial stresses can be determined using the following equation.

$$\sigma_f^D = \frac{E_f}{E_c}\sigma \tag{8}$$

$$\sigma_m^D = \frac{E_m}{E_c}\sigma \tag{9}$$

2.2 Upstream stresses

The upstream region III as shown in **Figure 1** is so far away from the crack tip that the stress and strain fields are also uniform. The axial stress of the fiber and the matrix can be determined using the following equations.

$$\sigma_f^U = \frac{E_f}{E_c}\sigma \tag{10}$$
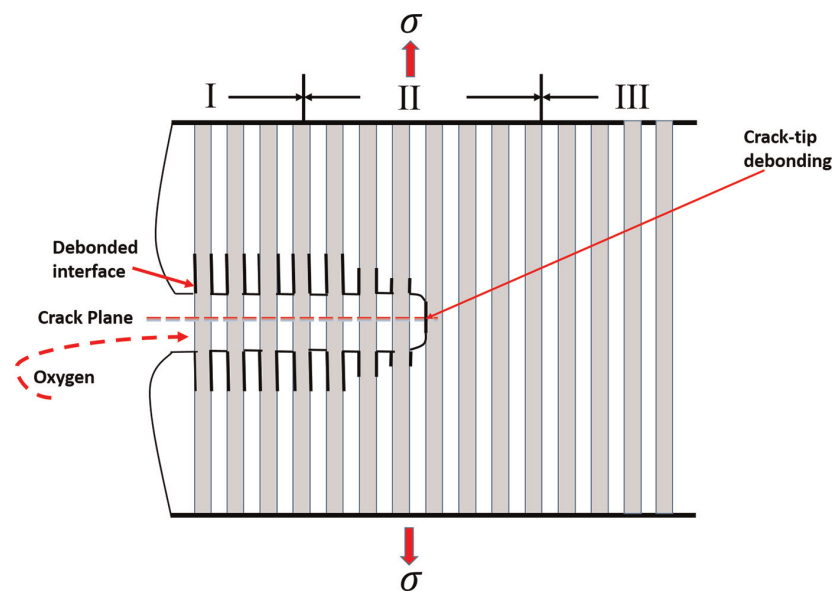
$$\sigma_m^U = \frac{E_m}{E_c}\sigma \tag{11}$$

Figure 1.
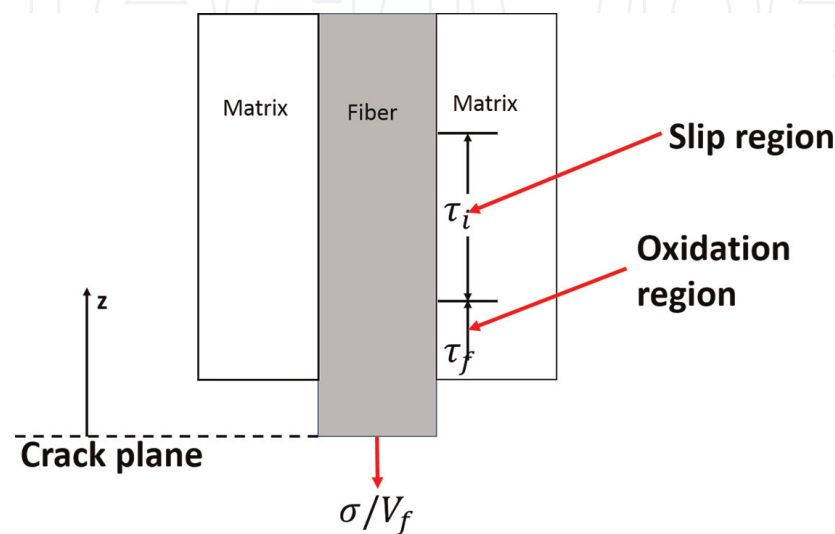*The schematic of crack-tip, interface debonding and oxidation.*

Figure 2.
The schematic of shear-lag model considering the interface oxidation and debonding.

2.3 Interface debonding

The fracture mechanics approach is used to determine the fiber/matrix interface debonding length [14].

$$\xi_d = -\frac{F}{4\pi r_f}\frac{\partial w_f(0)}{\partial l_d} - \frac{1}{2}\int_0^{l_d}\tau_i\frac{\partial v(z)}{\partial l_d}dz \tag{12}$$

where $F(=\pi r_f^2\sigma/V_f)$ denotes the fiber load at the matrix cracking plane, $w_f(0)$ denotes the fiber axial displacement on the matrix cracking plane, and $v(z)$ denotes the relative displacement between the fiber and the matrix. Substituting $w_f(z=0)$ and $v(z)$ into Eq. (12), it leads to the form of Eq. (13).

$$\frac{E_c\tau_i^2}{r_f V_m E_f E_m}(l_d-\zeta)^2 + \frac{2E_c\tau_f\tau_i}{r_f V_m E_f E_m}\zeta(l_d-\zeta) - \frac{\sigma\tau_i}{2V_f E_f}(l_d-\zeta) - \frac{T\tau_i}{2E_f}(l_d-\zeta)$$

$$+\frac{r_f\sigma T}{4V_f E_f} - \frac{r_f\sigma^2}{4V_f E_c} - \frac{\tau_f\sigma\zeta}{2V_f E_f} - \frac{\tau_f T}{2E_f}\zeta + \frac{E_c\tau_f^2}{r_f V_m E_f E_m}\zeta^2 - \xi_d = 0 \tag{13}$$

Solving Eq. (13), the fiber/matrix interface debonding length is determined by Eq. (14).

$$l_d = \left(1-\frac{\tau_f}{\tau_i}\right)\zeta + \frac{r_f V_m E_m}{4E_c\tau_i}\left(\frac{\sigma}{V_f}+T\right) - \left\{\frac{r_f^2 V_m E_m T^2}{4E_c\tau_i^2}\left[\frac{V_m E_m}{4E_c}\left(\frac{\sigma}{V_f T}+1\right)^2\right.\right.$$

$$\left.\left.+\frac{V_f E_f}{E_c}\left(\frac{\sigma}{V_f T}\right)^2 - \frac{\sigma}{V_f T}\right] + \frac{r_f V_m E_f E_m}{E_c\tau_i^2}\xi_d\right\}^{\frac{1}{2}} \tag{14}$$

2.4 Matrix cracking stress

The energy relationship to evaluate the steady-state matrix cracking stress is determined by Eq. (15) [4].

$$\frac{1}{2}\int_{-\infty}^{\infty}\left[\frac{V_f}{E_f}\left(\sigma_f^U-\sigma_f^D\right)^2 + \frac{V_m}{E_m}\left(\sigma_m^U-\sigma_m^D\right)^2\right]dz + \frac{1}{2\pi R^2 G_m}\int_{-l_d}^{l_d}\int_{r_f}^{R}\left(\frac{r_f\tau_i(z)}{r}\right)2\pi r dr dz$$

$$= V_m\xi_m + \left(\frac{4V_f l_d}{r_f}\right)\xi_d \tag{15}$$

where ξ_m is the matrix fracture energy and G_m is the matrix shear modulus. Substituting the fiber and matrix axial stresses in Eqs. (6)–(11) and the fiber/matrix interface debonding length of Eq. (14) into Eq. (15), the energy balance equation leads to the form of the following equation.

$$\eta_1\sigma^2 + \eta_2\sigma + \eta_3 = 0 \tag{16}$$

where

$$\eta_1 = \frac{l_d}{E_c} \tag{17}$$

$$\eta_2 = -\frac{2V_f T l_d}{E_c} \tag{18}$$

$$\eta_3 = \frac{V_f l_d T^2}{E_f} - \frac{V_f}{E_f}\left(\frac{2\tau_f}{r_f}\right)\zeta(2l_d - \zeta)T - \frac{V_f}{E_f}\left(\frac{2\tau_i}{r_f}\right)(l_d - \zeta)^2 T$$

$$+ \frac{4}{3}\left(\frac{V_f E_c}{V_m E_f E_m}\right)\left(\frac{\tau_i}{r_f}\right)^2\left[(l_d - \zeta)^3 + \left(\frac{\tau_f}{\tau_i}\right)^2\zeta^3\right] + \left(\frac{4V_f E_c}{V_m E_f E_m}\right)\frac{\tau_f \tau_i}{r_f^2}\zeta(l_d - \zeta)$$

$$\times\left[l_d - \left(1 - \frac{\tau_f}{\tau_i}\right)\zeta\right] - V_m \xi_m - \left(\frac{4V_f l_d}{r_f}\right)\xi_d$$

$$\tag{19}$$

3. Result and discussion

The effects of fiber volume, fiber/matrix interface debonding energy, interface shear stress, fiber strength, and oxidation temperature on the matrix cracking stress, interface oxidation, and interface debonding are analyzed.

3.1 Effect of the fiber volume on matrix cracking stress

The matrix cracking stress, fiber/matrix interface debonding length, and fiber/matrix interface oxidation length versus the oxidation time curves corresponding to different fiber volume of V_f = 30% and 35% are shown in **Figure 3**. When the fiber volume increases, the matrix cracking stress and the fiber/matrix interface oxidation length increase, and the fiber/matrix interface debonding length decreases.

When the fiber volume is V_f = 30%, the matrix cracking stress decreases from σ_{mc} = 86 to 44 MPa after t = 10 h oxidation at elevated temperature of T_{em} = 800°C; the fiber/matrix interface debonding length first decreases from l_d/r_f = 6.9 to 6.7 after t = 2 h oxidation at elevated temperature of T_{em} = 800°C and then increases to l_d/r_f = 9.0 after t = 10 h oxidation at elevated temperature of T_{em} = 800°C, and the fiber/matrix interface oxidation length increases from ζ/l_d = 0 to 0.94 after t = 10 h oxidation at elevated temperature of T_{em} = 800°C.

When the fiber volume is V_f = 35%, the matrix cracking stress decreases from σ_{mc} = 97 to 50 MPa after t = 10 h oxidation at elevated temperature of T_{em} = 800°C; the fiber/matrix interface debonding length first decreases from l_d/r_f = 5.8 to 5.7 after t = 1.7 h oxidation at elevated temperature of T_{em} = 800°C and then increases to l_d/r_f = 8.4 after t = 10 h oxidation at elevated temperature of T_{em} = 800°C, and the fiber/matrix interface oxidation length increases from ζ/l_d = 0 to 1.0 after t = 10 h oxidation at elevated temperature of T_{em} = 800°C.

3.2 Effect of the fiber/matrix interface debonding energy on matrix cracking stress

The matrix cracking stress, fiber/matrix interface debonding length, and fiber/matrix interface oxidation length versus the oxidation time curves corresponding to different interface debonding energies of ξ_d/ξ_m = 0.1 and 0.2 are shown in **Figure 4**. When the fiber/matrix interface debonding energy increases, the matrix cracking stress and the interface oxidation length increase, and the interface debonding length decreases.

When the fiber/matrix interface debonding energy is ξ_d/ξ_m = 0.1, the matrix cracking stress decreases from σ_{mc} = 86 MPa to 32 MPa after t = 10 h oxidation at elevated temperature of T_{em} = 800°C; the fiber/matrix interface debonding length
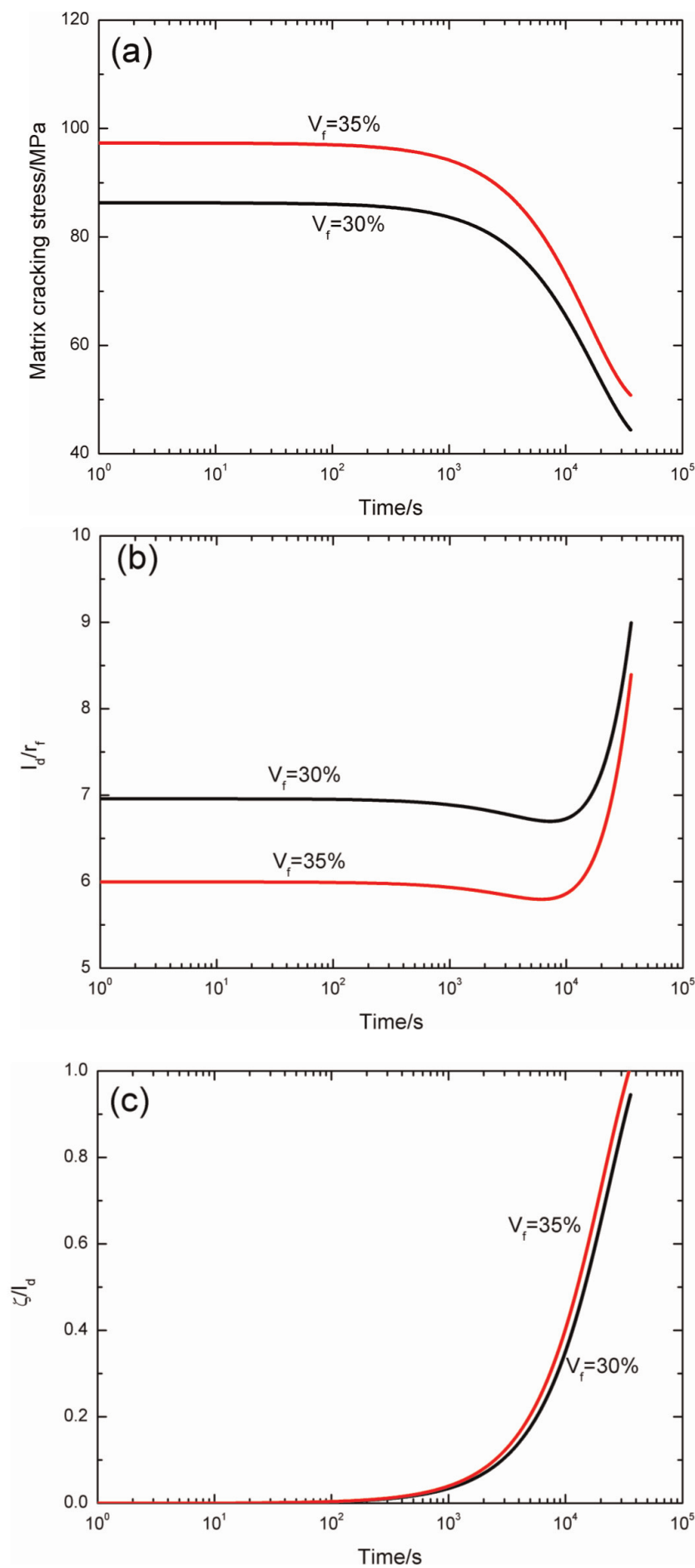
Figure 3.
(a) The matrix cracking stress versus the oxidation time, (b) the fiber/matrix interface debonding length versus the oxidation time, and (c) the fiber/matrix interface oxidation length versus the oxidation time corresponding to different fiber volume of V_f = 30 and 35%.
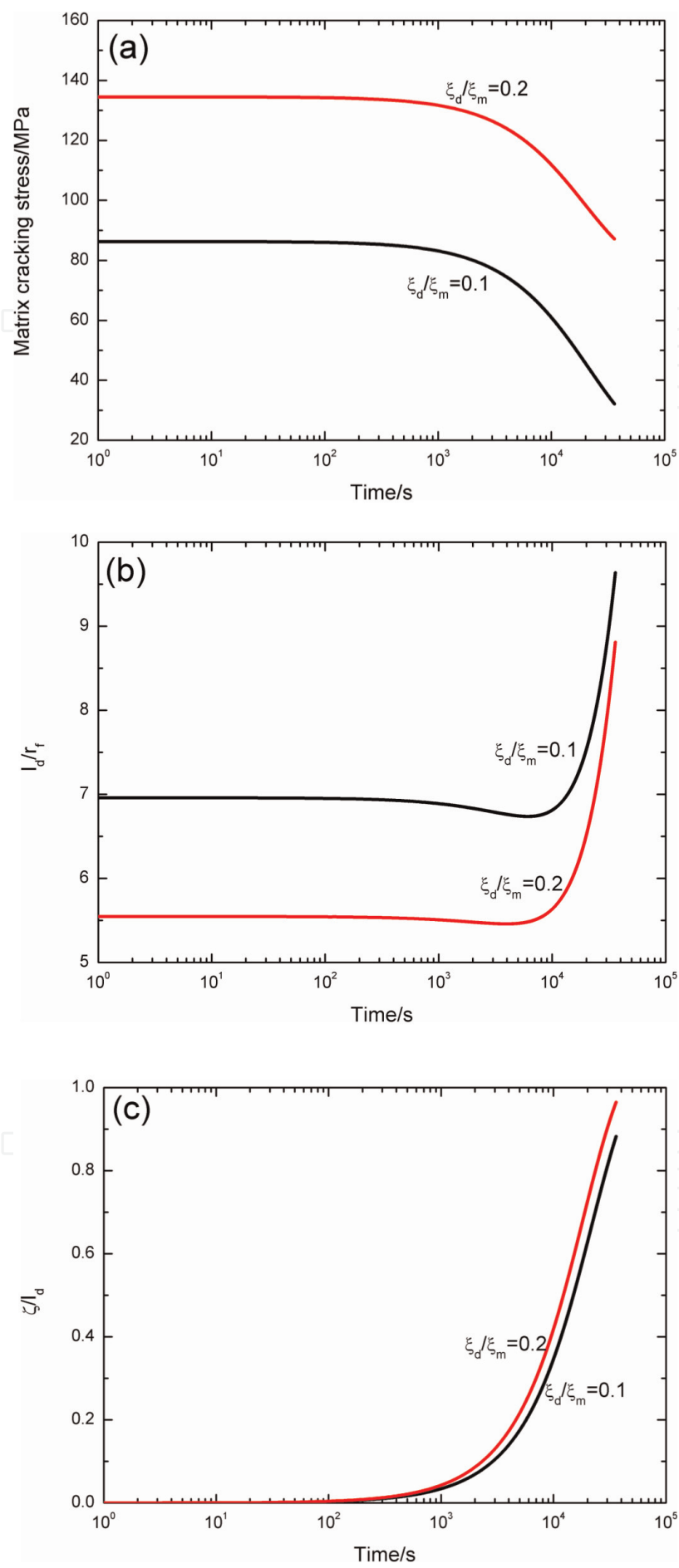
Figure 4.
(a) The matrix cracking stress versus the oxidation time, (b) the fiber/matrix interface debonding length versus the oxidation time, and (c) the fiber/matrix interface oxidation length versus the oxidation time corresponding to different interface debonding energy of ξ_d/ξ_m = 0.1 and 0.2.

first decreases from l_d/r_f = 6.9 to 6.7 after t = 1.7 h oxidation at elevated temperature of T_{em} = 800°C and then increases to l_d/r_f = 9.6 after t = 10 h oxidation at elevated temperature of T_{em} = 800°C, and the fiber/matrix interface oxidation length increases from ζ/l_d = 0 to 0.88 after t = 10 h oxidation at elevated temperature of T_{em} = 800°C.

When the fiber/matrix interface debonding energy is ξ_d/ξ_m = 0.2, the matrix cracking stress decreases from σ_{mc} = 134 to 87 MPa after t = 10 h oxidation at elevated temperature of T_{em} = 800°C; the fiber/matrix interface debonding length first decreases from l_d/r_f = 5.5 to 5.4 after t = 1.1 h oxidation at elevated temperature of T_{em} = 800°C and then increases to l_d/r_f = 8.8 after t = 10 h oxidation at elevated temperature of T_{em} = 800°C, and the fiber/matrix interface oxidation length increases from ζ/l_d = 0 to 0.96 after t = 10 h oxidation at elevated temperature of T_{em} = 800°C.

3.3 Effect of the fiber/matrix interface shear stress on the matrix cracking stress

The matrix cracking stress, fiber/matrix interface debonding length, and the fiber/matrix interface oxidation length versus the oxidation time curves corresponding to different fiber/matrix interface shear stress of τ_i = 20 and 10 MPa are shown in **Figure 5**. When the fiber/matrix interface shear stress in the slip region increases, the matrix cracking stress and the fiber/matrix interface oxidation length increase, and the fiber/matrix interface debonding length decreases.

When the fiber/matrix interface shear stress is τ_i = 10 MPa, the matrix cracking stress decreases from σ_{mc} = 67 to 43 MPa after t = 10 h oxidation at elevated temperature of T_{em} = 800°C; the fiber/matrix interface debonding length first decreases from l_d/r_f = 8.0 to 7.7 after t = 2.6 h oxidation at elevated temperature of T_{em} = 800°C and then increases to l_d/r_f = 9.1 after t = 10 h oxidation at elevated temperature of T_{em} = 800°C, and the fiber/matrix interface oxidation length increases from ζ/l_d = 0 to 0.93 after t = 10 h oxidation at elevated temperature of T_{em} = 800°C.

When the fiber/matrix interface shear stress is τ_i = 20 MPa, the matrix cracking stress decreases from σ_{mc} = 102 to 45 MPa after t = 10 h oxidation at elevated temperature of T_{em} = 800°C; the fiber/matrix interface debonding length first decreases from l_d/r_f = 6.2 to 6.0 after t = 1.7 h oxidation at elevated temperature of T_{em} = 800°C and then increases to l_d/r_f = 8.9 after t = 10 h oxidation at elevated temperature of T_{em} = 800°C, and the fiber/matrix interface oxidation length increases from ζ/l_d = 0 to 0.95 after t = 10 h oxidation at elevated temperature of T_{em} = 800°C.

The matrix cracking stress, fiber/matrix interface debonding length, and the fiber/matrix interface oxidation length versus the oxidation time curves corresponding to different fiber/matrix interface shear stress of τ_f = 1 and 5 MPa are shown in **Figure 6**. When the fiber/matrix interface shear stress in the oxidation region increases, the matrix cracking stress and the fiber/matrix interface oxidation length increase, and the fiber/matrix interface debonding length decreases.

When the fiber/matrix interface shear stress is τ_f = 1 MPa, the matrix cracking stress decreases from σ_{mc} = 86 to 28 MPa after t = 10 h oxidation at elevated temperature of T_{em} = 800°C; the fiber/matrix interface debonding length first decreases from l_d/r_f = 6.9 to 6.7 after t = 1.6 h oxidation at elevated temperature of T_{em} = 800°C and then increases to l_d/r_f = 9.8 after t = 10 h oxidation at elevated temperature of T_{em} = 800°C, and the fiber/matrix interface oxidation length increases from ζ/l_d = 0 to 0.86 after t = 10 h oxidation at elevated temperature of T_{em} = 800°C.
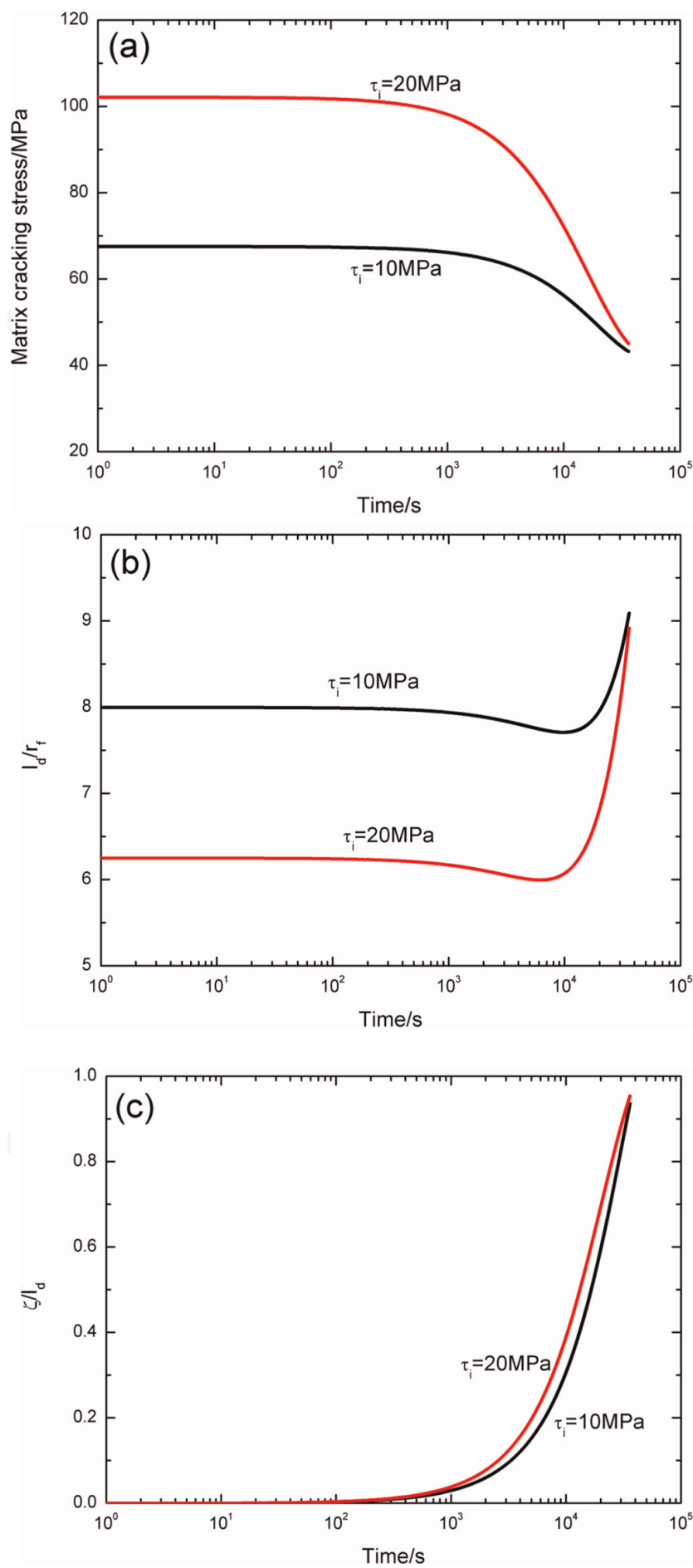
Figure 5.
(a) The matrix cracking stress versus the oxidation time, (b) the fiber/matrix interface debonding length versus the oxidation time, and (c) the fiber/matrix interface oxidation length versus the oxidation time corresponding to different interface shear stress of $\tau_i = 10$ and 20 MPa.
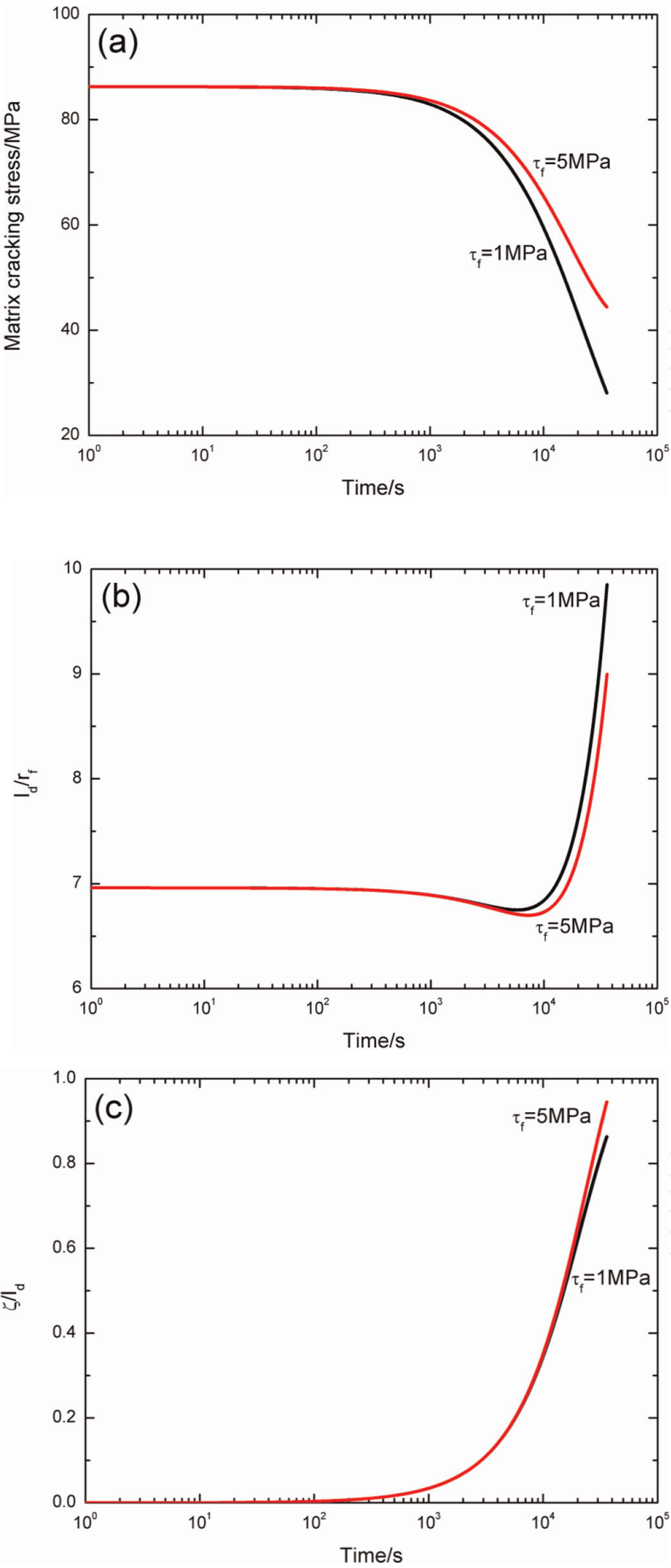
Figure 6.
(a) The matrix cracking stress versus the oxidation time, (b) the fiber/matrix interface debonding length versus oxidation time, and (c) the fiber/matrix interface oxidation length versus the oxidation time corresponding to different interface shear stress of $\tau_f = 1$ and 5 MPa.

When the fiber/matrix interface shear stress is τ_f = 5 MPa, the matrix cracking stress decreases from σ_{mc} = 86 to 44 MPa after t = 10 h oxidation at elevated temperature of T_{em} = 800°C; the fiber/matrix interface debonding length first decreases from l_d/r_f = 6.9 to 6.7 after t = 2 h oxidation at elevated temperature of T_{em} = 800°C and then increases to l_d/r_f = 9 after t = 10 h oxidation at elevated temperature of T_{em} = 800°C, and the fiber/matrix interface oxidation length increases from ζ/l_d = 0 to 0.94 after t = 10 h oxidation at elevated temperature of T_{em} = 800°C.

3.4 Effect of the fiber strength on matrix cracking stress

The matrix cracking stress, fiber/matrix interface debonding length, and fiber/matrix interface oxidation length versus the oxidation time curves corresponding to different fiber strength of σ_0 = 1 and 2 GPa are shown in **Figure 7**. When the fiber strength increases, the matrix cracking stress and the fiber/matrix interface debonding length increase, and the fiber/matrix interface oxidation length decreases.

When the fiber strength is σ_0 = 1 GPa, the matrix cracking stress decreases from σ_{mc} = 38 to 18 MPa after t = 10 h oxidation at elevated temperature of T_{em} = 800°C; the fiber/matrix interface debonding length first decreases from l_d/r_f = 14.9 to 14.7 after t = 2 h oxidation at elevated temperature of T_{em} = 800°C and then increases to l_d/r_f = 16.3 after t = 10 h oxidation at elevated temperature of T_{em} = 800°C, and the fiber/matrix interface oxidation length increases from ζ/l_d = 0 to 0.52 after t = 10 h oxidation at elevated temperature of T_{em} = 800°C.

When the fiber strength is σ_0 = 2 GPa, the matrix cracking stress decreases from σ_{mc} = 43 to 21 MPa after t = 10 h oxidation at elevated temperature of T_{em} = 800°C; the fiber/matrix interface debonding length first decreases from l_d/r_f = 15.3 to 15.2 after t = 2.3 h oxidation at elevated temperature of T_{em} = 800°C and then increases to l_d/r_f = 16.6 after t = 10 h oxidation at elevated temperature of T_{em} = 800°C, and the fiber/matrix interface oxidation length increases from ζ/l_d = 0 to 0.51 after t = 10 h oxidation at elevated temperature of T_{em} = 800°C.

3.5 Effect of the temperature on matrix cracking stress

The matrix cracking stress, fiber/matrix interface debonding length, and fiber/matrix interface oxidation length versus the oxidation time curves corresponding to different oxidation temperature of T_{em} = 600 and 800°C are shown in **Figure 8**. When the oxidation temperature increases, the matrix cracking stress decreases, and the fiber/matrix interface oxidation length and the interface debonding length increase.

When the oxidation temperature is T_{em} = 600°C, the matrix cracking stress decreases from σ_{mc} = 86.3 to 73 MPa after t = 10 h oxidation; the fiber/matrix interface debonding length decreases from l_d/r_f = 6.9 to 6.7 after t = 10 h oxidation, and the fiber/matrix interface oxidation length increases from ζ/l_d = 0 to 0.19 after t = 10 h oxidation.

When the oxidation temperature is T_{em} = 800°C, the matrix cracking stress decreases from σ_{mc} = 86 to 44 MPa after t = 10 h oxidation; the fiber/matrix interface debonding length first decreases from l_d/r_f = 6.9 to 6.7 after t = 2 h oxidation and then increases to l_d/r_f = 9 after t = 10 h oxidation, and the fiber/matrix interface oxidation length increases from ζ/l_d = 0 to 0.94 after t = 10 h oxidation.
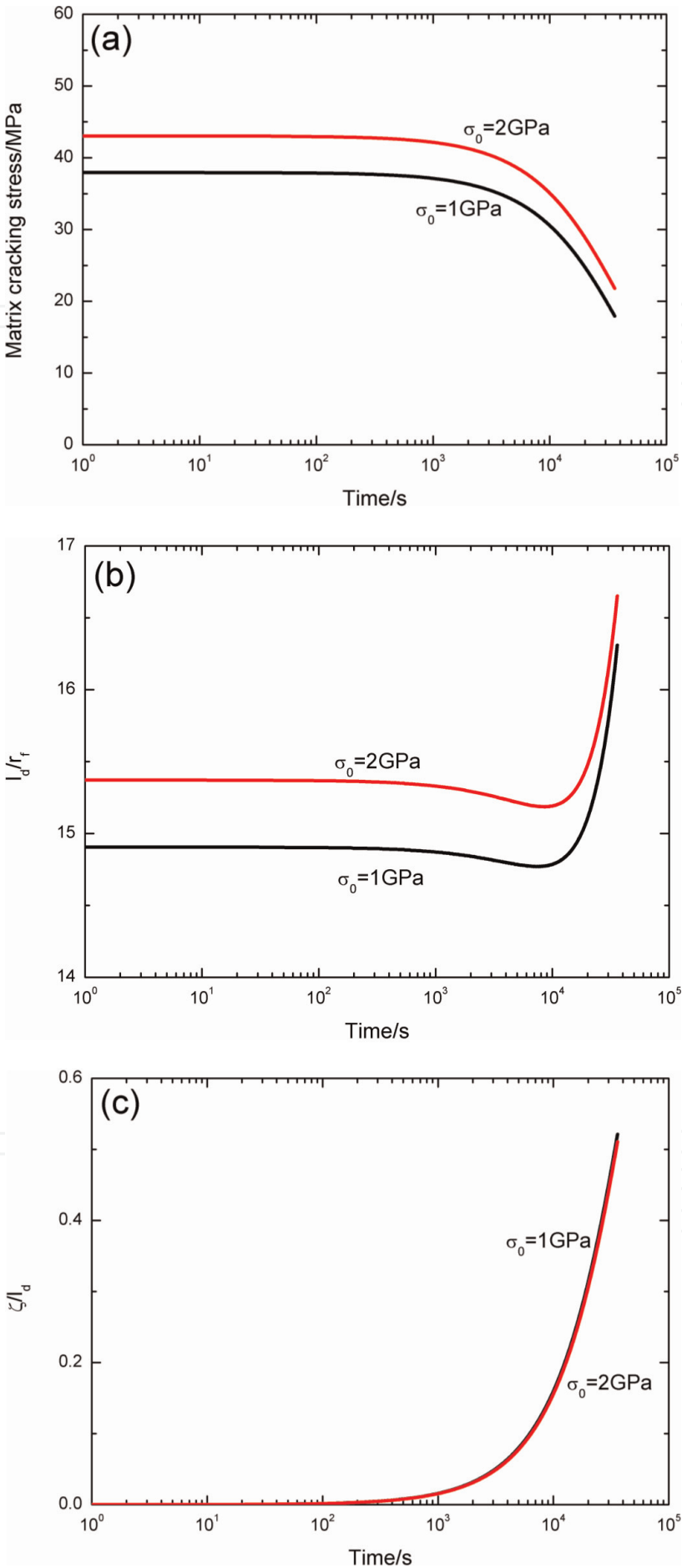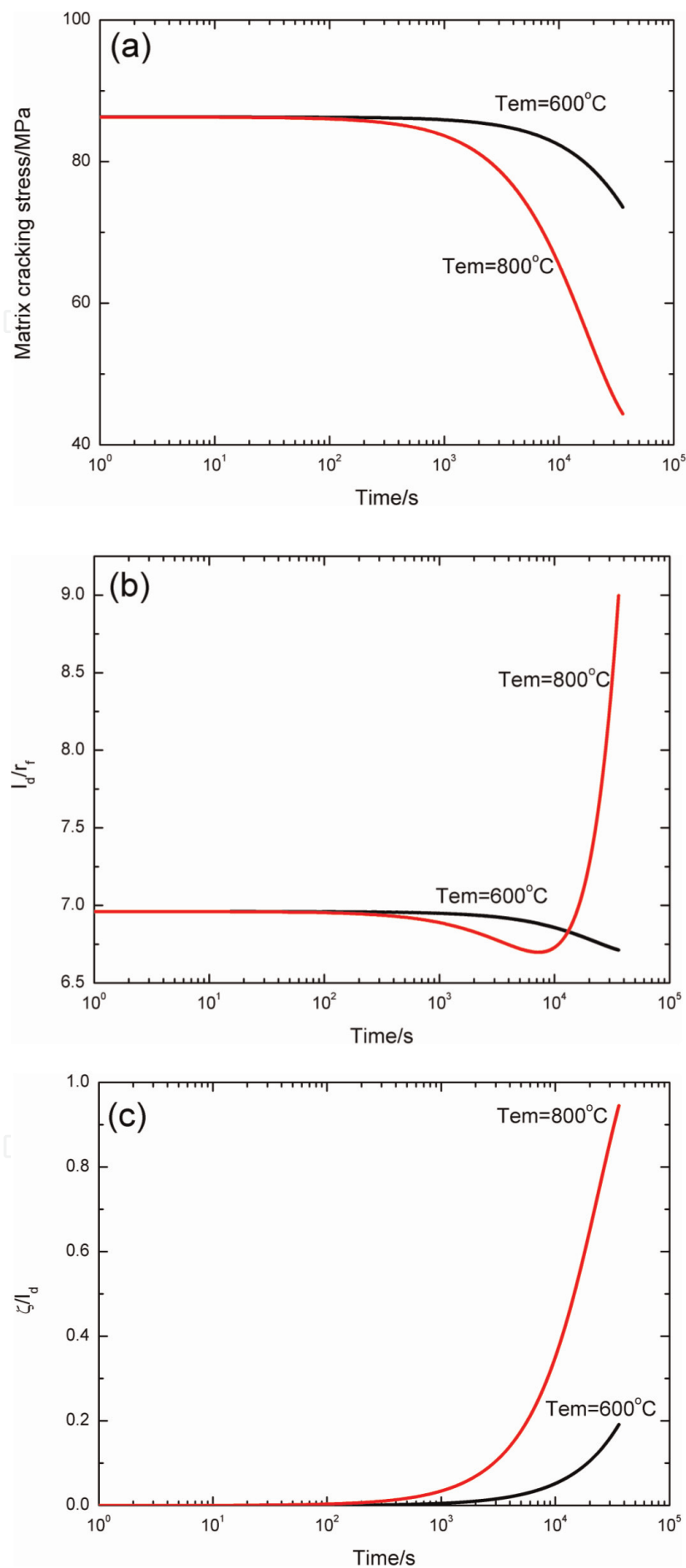
Figure 7.
(a) The matrix cracking stress versus the oxidation time, (b) the fiber/matrix interface debonding length versus the oxidation time, and (c) the fiber/matrix interface oxidation length versus the oxidation time corresponding to different fiber strength of σ₀ = 1 and 2 GPa.

Figure 8.
(a) The matrix cracking stress versus the oxidation time, (b) the fiber/matrix interface debonding length versus the oxidation time, and (c) the fiber/matrix interface oxidation length versus the oxidation time corresponding to different oxidation temperature of T_{em} = 600 and 800°C.

4. Experimental comparison

Barsoum et al. [15] investigated the matrix crack initiation in fiber-reinforced CMCs. The experimental and predicted matrix cracking stress versus the fiber volume corresponding to different fiber/matrix interface debonding energy of SiC/borosilicate, SiC/LAS, and C/borosilicate composites is shown in **Figures 9–11**.

For the SiC/borosilicate composite, the predicted matrix cracking stress with the fiber/matrix interface debonding energy range of ξ_d/ξ_m = 0.05, 0.1, and 0.2 agrees with the experimental data corresponding to the fiber volume changing from 10 to 50%, as shown in **Figure 9**. When the fiber/matrix interface debonding energy is ξ_d/ξ_m = 0.05, the matrix cracking stress increases from σ_{mc} = 49.4 MPa at the fiber volume of V_f = 10% to σ_{mc} = 334 MPa at the fiber volume of V_f = 50%; when the fiber/matrix interface debonding energy is ξ_d/ξ_m = 0.1, the matrix cracking stress increases from σ_{mc} = 52.2 MPa at the fiber volume of V_f = 10% to σ_{mc} = 371 MPa at the fiber volume V_f = 50%; and when the fiber/matrix interface debonding energy is ξ_d/ξ_m = 0.2, the matrix cracking stress increases from σ_{mc} = 57.1 MPa at the fiber volume of V_f = 10% to σ_{mc} = 428 MPa at the fiber volume of V_f = 50%.

For the SiC/LAS composite, the matrix cracking stress with the interface debonding energy range of ξ_d/ξ_m = 0.01, 0.02, and 0.03 agrees with the experimental data corresponding to the fiber volume changing from 30 to 50%, as shown in **Figure 10**. When the fiber/matrix interface debonding energy is ξ_d/ξ_m = 0.01, the matrix cracking stress increases from σ_{mc} = 228 MPa at the fiber volume of V_f = 30% to σ_{mc} = 423 MPa at the fiber volume of V_f = 50%; when the fiber/matrix interface debonding energy is ξ_d/ξ_m = 0.02, the matrix cracking stress increases from σ_{mc} = 257 MPa at the fiber volume of V_f = 30% to σ_{mc} = 489 MPa at the fiber volume of V_f = 50%; and when the fiber/matrix interface debonding energy is ξ_d/ξ_m = 0.03, the matrix cracking stress increases from σ_{mc} = 281 MPa at the fiber volume of V_f = 30% to σ_{mc} = 542 MPa at the fiber volume of V_f = 50%.

For the C/borosilicate composite, the predicted matrix cracking stress with the fiber/matrix interface debonding energy range of ξ_d/ξ_m = 0.01, 0.02, and 0.03
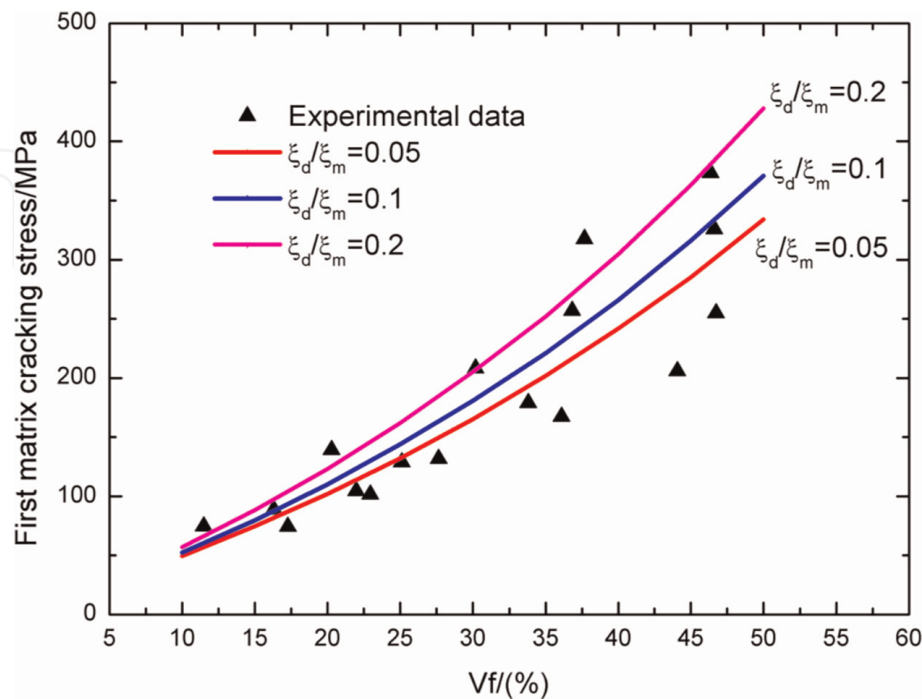

Figure 9.
The experimental and predicted matrix cracking stress versus the fiber volume corresponding to different fiber/matrix interface debonding energy of SiC/borosilicate composite.
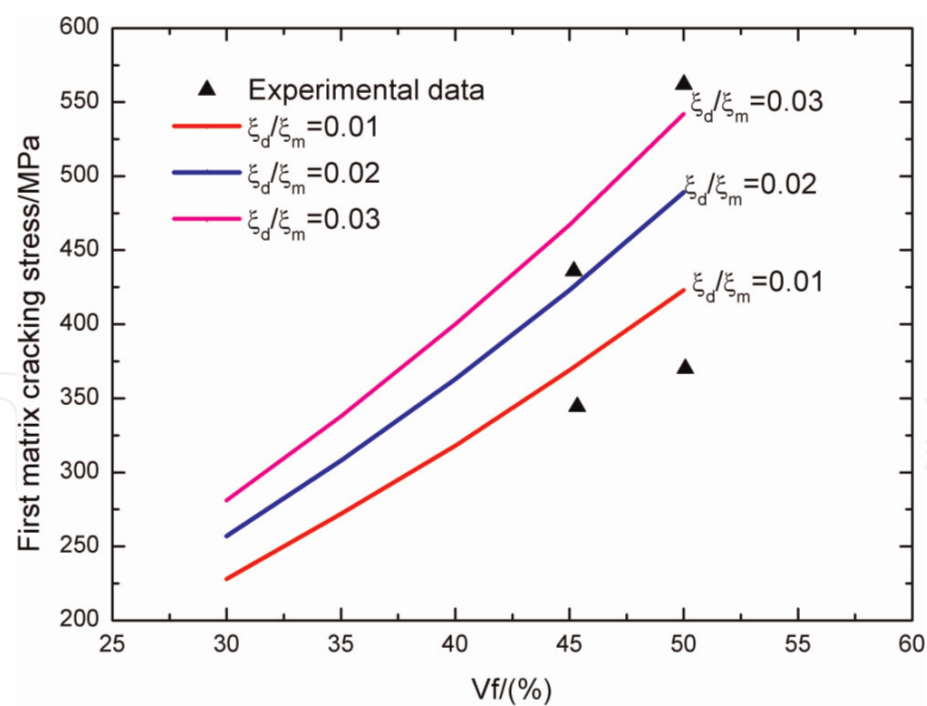
Figure 10.
The experimental and predicted matrix cracking stress versus the fiber volume corresponding to different fiber/ matrix interface debonding energy of SiC/LAS composite.
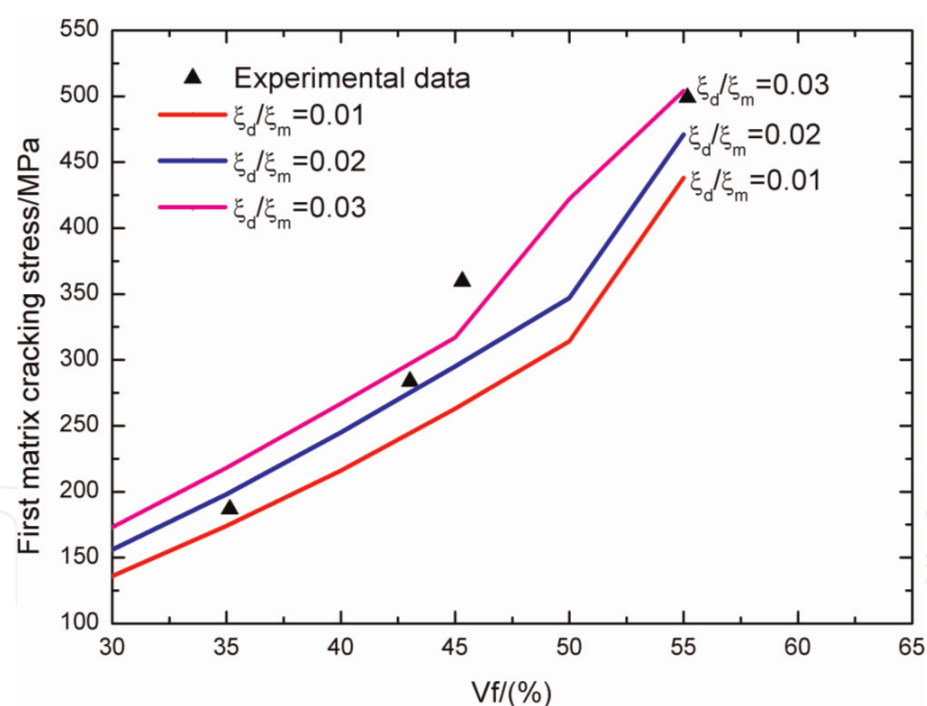

Figure 11.
The experimental and predicted matrix cracking stress versus the fiber volume corresponding to different fiber/ matrix interface debonding energy of C/borosilicate composite.

agrees with the experimental data corresponding to the fiber volume changing from 30 to 55%, as shown in **Figure 11**. When the fiber/matrix interface debonding energy is $\xi_d/\xi_m = 0.01$, the matrix cracking stress increases from $\sigma_{mc} = 136$ MPa at the fiber volume of $V_f = 30\%$ to $\sigma_{mc} = 438$ MPa at the fiber volume of $V_f = 55\%$; when the fiber/matrix interface debonding energy is $\xi_d/\xi_m = 0.02$, the matrix cracking stress increases from $\sigma_{mc} = 156$ MPa at the fiber volume of $V_f = 30\%$ to $\sigma_{mc} = 471$ MPa at the fiber volume of $V_f = 55\%$; and when the fiber/matrix interface

debonding energy is $\xi_d/\xi_m = 0.03$, the matrix cracking stress increases from $\sigma_{mc} = 173$ MPa at the fiber volume of $V_f = 30\%$ to $\sigma_{mc} = 504$ MPa at the fiber volume of $V_f = 55\%$.

Yang [16] investigated the mechanical behavior of C/SiC composite after unstressed oxidation at elevated temperature of 700°C in air atmosphere. The composite was divided into two types based on the interface bonding, i.e., strong interface bonding and weak interface bonding. For the C/SiC with the strong interface bonding, the matrix cracking stresses of C/SiC corresponding to the proportional limit stresses in the tensile curves are 37, 30, and 20 MPa corresponding to the cases of without oxidation, 4 h oxidation, and 6 h unstressed oxidation, respectively. For the C/SiC with the weak interface bonding, the matrix cracking stresses
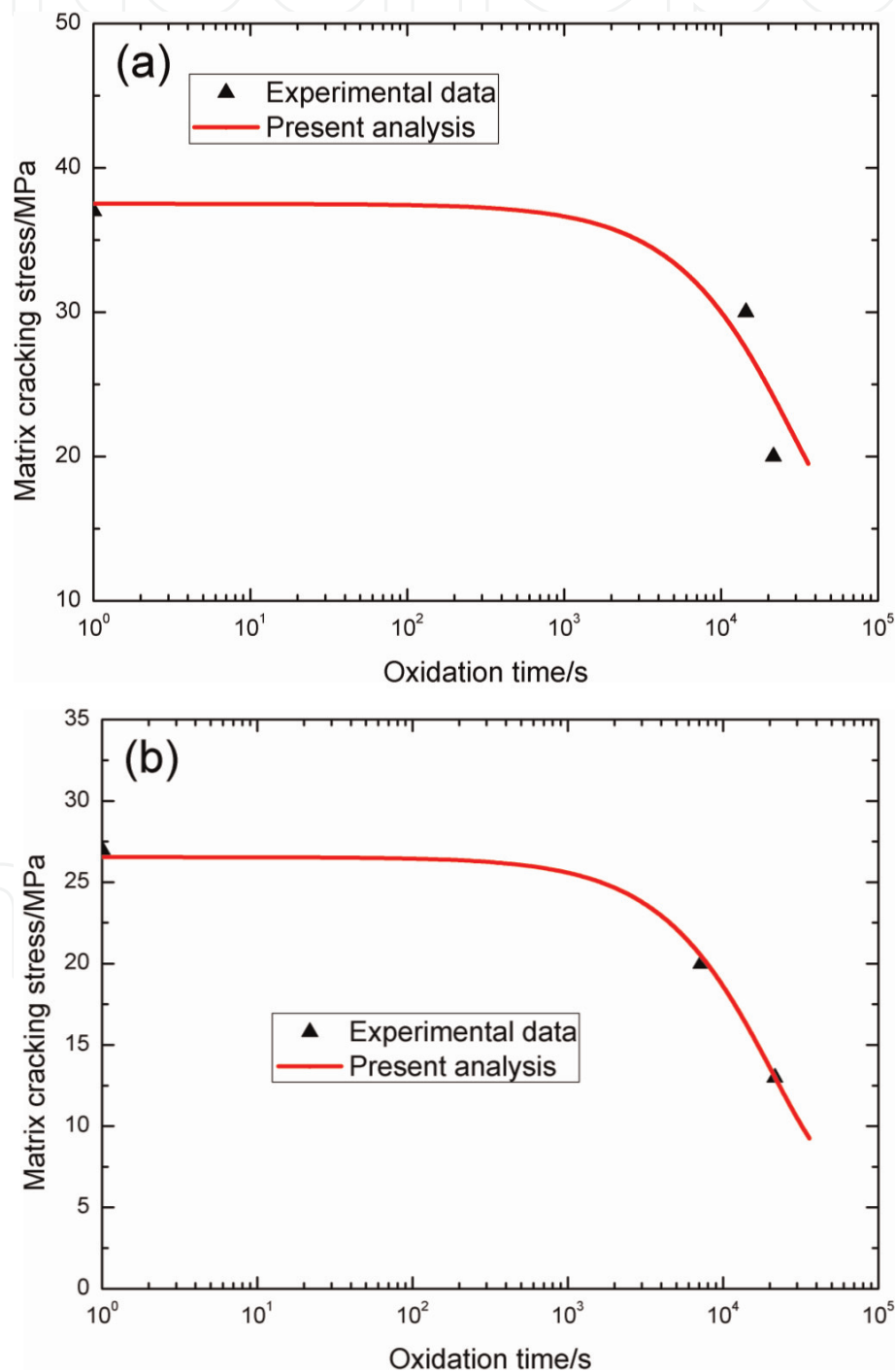

Figure 12.
The experimental and predicted matrix cracking stress versus the oxidation time of C/SiC composite after unstressed oxidation at 700°C in air corresponding to (a) strong interface bonding and (b) weak interface bonding.

of C/SiC corresponding to the proportional limit stresses in the tensile curves are 27, 20, and 13 MPa corresponding to the cases of without oxidation, 2 h oxidation, and 6 h unstressed oxidation, respectively. The experimental and predicted matrix cracking stresses of C/SiC composite with strong and weak interface bonding after unstressed oxidation at elevated temperature of 700°C in air are shown in **Figure 12a** and **b**, respectively. The matrix cracking stress decreases 18.9% after oxidation for 4 h, 46% after oxidation for 6 h for C/SiC with strong interface bonding, 25.9% after oxidation for 1 h, and 51.8% after oxidation for 6 h for C/SiC with weak interface bonding. The theoretical predicted results agreed with experimental data. The strong interface bonding can be used for oxidation resistant of C/SiC composite at elevated temperature.

5. Conclusion

In this chapter, the time-dependent matrix cracking of fiber-reinforced CMCs was investigated using the energy balance approach. The relationship between the matrix cracking stress, fiber and interface oxidation, and fiber failure was established. The effects of the fiber volume, interface shear stress and interface debonding energy, fiber failure, and oxidation temperature on the time-dependent matrix cracking stress were analyzed. The experimental matrix cracking stress of different fiber-reinforced CMCs was predicted.

1. When the fiber volume, fiber/matrix interface debonding energy and interface shear stress increase, the matrix cracking stress and the fiber/matrix interface oxidation length increase, and the fiber/matrix interface debonding length decreases.

2. When the fiber strength increases, the matrix cracking stress and the fiber/matrix interface debonding length increase, and the fiber/matrix interface oxidation length decreases.

3. When the oxidation temperature increases, the matrix cracking stress decreases, and the fiber/matrix interface oxidation length and the interface debonding length increase.

Acknowledgements

Author details

Li Longbiao
College of Civil Aviation, Nanjing University of Aeronautics and Astronautics,
Nanjing, P.R. China

*Address all correspondence to: llb451@nuaa.edu.cn

IntechOpen

References

[1] Li L. Damage, Fracture and Fatigue of Ceramic-Matrix Composites. Singapore: Springer Nature Singapore Pte Ltd.; 2018. DOI: 10.1007/978-981-13-1783-5. ISBN: 978-981-13-1782-8

[2] Li L. Thermomechanical Fatigue of Ceramic-Matrix Composites. New Jersey, USA: Wiley-VCH; 2019. ISBN: 978-3-527-34637-0. Available from: https://onlinelibrary.wiley.com/doi/book/10.1002/9783527822614

[3] Aveston J, Cooper GA, Kelly A. Single and multiple fracture. In: The Properties of Fiber Composites, Conference on Proceedings. National Physical Laboratory, Guildford: IPC Science and Technology Press; 1971. pp. 15-26

[4] Budiansky B, Hutchinson JW, Evans AG. Matrix fracture in fiber-reinforced ceramics. Journal of the Mechanics and Physics of Solids. 1986;**34**(2):167-189

[5] Rajan VP, Zok FW. Matrix cracking of fiber-reinforced ceramic composites in shear. Journal of the Mechanics and Physics of Solids. 2014;**73**:3-21

[6] Li L. Modeling first matrix cracking stress of fiber-reinforced ceramic-matrix composites considering fiber fracture. Theoretical and Applied Fracture Mechanics. 2017;**92**:24-32

[7] Li L. Time-dependent damage and fracture of fiber-reinforced ceramic-matrix composites at elevated temperatures. Composite Interfaces. 2019;**26**(11):963-988. DOI: 10.1080/09276440.2019.1569397

[8] Marshall DB, Cox BN, Evans AG. The mechanics of matrix cracking in brittle matrix composites. Acta Metallurgica et Materialia. 1985;**33**(11):2013-2021

[9] McCartney LN. Mechanics of matrix cracking in brittle-matrix fiber-reinforced composites. Proceedings of the Royal Society of London. 1987;**A409**:329-350

[10] Halbig MC, McGuffin-Cawley JM, Eckel AJ, Brewer DN. Oxidation kinetics and stress effects for the oxidation of continuous carbon fibers within a microcracked C/SiC ceramic matrix composite. Journal of the American Ceramic Society. 2008;**91**(2):519-526

[11] Casas L, Martinez-Esnaola JM. Modelling the effect of oxidation on the creep behavior of fiber-reinforced ceramic matrix composites. Acta Materialia. 2003;**51**(13):3745-3757

[12] Lara-Curzio E. Analysis of oxidation-assisted stress-rupture of continuous fiber-reinforced ceramic matrix composites at intermediate temperatures. Composites: Part A. 1999;**30**:549-554

[13] Curtin WA. Theory of mechanical properties of ceramic-matrix composites. Journal of the American Ceramic Society. 1991;**74**:2837-2845

[14] Gao YC, Mai YW, Cotterell B. Fracture of fiber-reinforced materials. Journal of Applied Mathematics and Physics. 1988;**39**(4):550-572

[15] Barsoum M, Kangutkar P, Wang A. Matrix cracking initiation in ceramic matrix composites, part I experiment and test results. Composites Science and Technology. 1992;**44**:257-269

[16] Yang CP. Mechanical characterization and oxidation damage modeling of ceramic matrix composites [PhD Thesis]. Xi'an: Northwestern Polytechnical University; 2011